Density Functional Study on the Carbostannylation of Aryne by the Palladium(0)−Iminophosphine Catalyst. Does the Apical Site Really Contribute to the Catalytic Reaction?

Toshiaki Matsubara*

Fukui Institute for Fundamental Chemistry, Kyoto University, 34-4 Takano-Nishihiraki-cho, Sakyo-ku, Kyoto 606-8103, Japan

Received May 29, 2003

The mechanism of carbostannylation of aryne by the palladium(0)−iminophosphine catalyst was examined using the density functional method (B3LYP) paying attention to the role of the apical site. The calculations showed that the catalytic reaction takes not cycle A but cycle B out of two possible cycles (cycle A: **1** → **3** → **1**; cycle B: **1** → **4** → **1**). It was found that the apical site is an origin of the catalysis of the palladium(0)−iminophosphine complex. The contribution of the apical site lowers the energy barrier of the rate-determining step and makes the catalytic reaction possible. The Sn−C σ-bond breaking of $SnH_3C{\equiv}CH$, which is a rate-determining step in cycle B, proceeds by the heterolytic mechanism without the oxidative addition of the Sn−C σ-bond to Pd (path b). However, when the Pd atom is replaced by the Pt atom, the homolytic cleavage of the Sn−C σ-bond with the oxidative addition to Pt (path c) becomes energetically more favorable.

Downloaded by CARLI CONSORTIUM on June 29, 2009
Published on September 16, 2003 on http://pubs.acs.org | doi: 10.1021/om0304053

1. Introduction

The insertion of arynes into the Sn−C σ-bond of alkynylstannanes is a useful method to generate various 1,2-disubstituted arenes. The first catalytic reaction of the carbostannylation of aryne was recently demonstrated by Yoshida et al.[1] using the palladium(0)−iminophosphine catalyst. This catalytic reaction has attracted much attention from many chemists as a convenient method to convert alkynylstannanes and aryne to a wide variety of *ortho*-substituted arylstannanes. This is also potentially applicable to the synthesis of biaryl compounds.[2] However, an examination to understand the details of the reaction mechanism is not developed at all, because most efforts of experimentalists have been devoted to the synthesis of the target compounds. The purpose of the present study is, therefore, to reveal the mechanism of the catalytic reaction and the origin of the novel catalysis of the palladium(0)−iminophosphine complex to support the molecular design of organic compounds.

The alternative catalytic cycles A and B are possible for the carbostannylation of aryne by the palladium(0)−iminophosphine complex as depicted in Figure 1.[1] Starting from the common palladium(0)−iminophosphine complex **1** with a vacant site, the reaction pathway separates into two mutually independent cycles. The selection of cycles A and B depends on the first incoming substrate, alkynylstannane or aryne. In cycle A, the first incoming alkynylstannane is attracted to the vacant site of the palladium(0)−iminophosphine complex **1**, and the Sn−C σ-bond is broken on the active site of the Pd atom. The separated SnR_3 and C≡CR′ have a bonding with the Pd by coordination. That is, the first half of the catalytic cycle is the oxidative addition of the Sn−C σ-bond of alkynylstannane to the palladium(0)−iminophosphine complex **1** in cycle A. In the second half of the catalytic cycle, the other substrate, aryne, approaches the intermediate **3** formed by the oxidative addition of the Sn−C σ-bond, and both SnR_3 and C≡CR′ coordinated to Pd are transferred to the triple bond of aryne. The 1,2-disubstituted arene is then finally released with the formation of the starting palladium(0)−iminophosphine complex **1**. On the other hand, in cycle B, the triple bond of the incoming aryne coordinates to the vacant site of **1** in the first step. In the second step, the formed C≡C π-complex **4** reacts with the next incoming alkynylstannane to produce the 1,2-disubstituted arene.

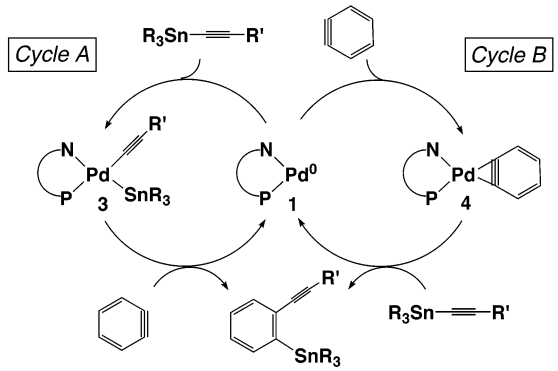

Figure 1. Proposed catalytic cycles A and B of carbostannylation of aryne by the palladium(0)−iminophosphine complex **1**.

(1) Yoshida, H.; Honda, Y.; Shirakawa, E.; Hiyama, T. *Chem. Commun.* **2001**, 1880.
(2) Farina, V.; Krishnamurthy, V.; Scott, W. J. *Org. React.* **1997**, *50*, 1.

10.1021/om0304053 CCC: $25.00 © 2003 American Chemical Society
Publication on Web 09/16/2003

Downloaded by CARLI CONSORTIUM on June 29, 2009
Published on September 16, 2003 on http://pubs.acs.org | doi: 10.1021/om0304053

In each cycle, it is clear that the second step is the key step to understand how the palladium−iminophosphine complex successfully completes the catalytic cycle. The active site of the palladium complex seems to be already fully occupied in both intermediates **3** and **4** at a glance. However, we should remember that the apical site of the palladium complex plays an important role in some cases, as the author has suggested.[3−7] In addition, the Sn−C σ-bond of alkynylstannane is highly polarized. We will know later that these two points are quite important to understand the peculiar catalysis of the palladium(0)−iminophosphine complex **1** for the carbostannylation of aryne.

In the present study, simple model substrates $SnH_3C{\equiv}CH$ as alkynylstannane and benzyne as aryne were adopted for the computation by the density functional method (B3LYP). The real ligand *N*-(2-diphenylphosphinobenzylidene)-2-phenylethylamine was modeled by replacing the substituents attached to the N and P atoms by H atoms. Following the explanation of the computational procedures, cycle A is first discussed in section 3.1. Cycle B, which is considered to be a real cycle, is discussed in detail in the subsequent section, 3.2. Conclusions are summarized in the last section.

2. Computational Procedures

All calculations were performed using the Gaussian98 program.[8] The calculations of energetics as well as geometry optimizations were carried out at the B3LYP level of theory, which consists of a hybrid Becke + Hartree−Fock exchange and a Lee−Yang−Parr correlation functional with nonlocal corrections.[9] In the geometry optimizations, the lanl2dz basis set, hereinafter referred to as BSI, was adopted for all the atoms. For three metals, Ni, Pd, and Pt, the basis set consists of the double-ζ valence basis functions and the relativistic effective core potential (ECP) determined by Hay−Wadt[10] to replace the core electrons except for the 18 electrons in the valence shell. For Sn, the double-ζ valence basis functions and the relativistic ECP[11] by Hay−Wadt to replace the core electrons up to the 4d orbital are employed. The higher basis set BSII including the polarization functions was used to obtain more reliable energies for the optimized structures with the basis set BSI. The basis set BSII is at the 6-31G** level for the H, C, N, and P atoms, and the double-ζ valence basis functions augmented by an additional single set of f orbitals with the exponents[12] 3.130(Ni), 1.472(Pd), and 0.993(Pt) and the Hay−Wadt ECP[10] to replace the core electrons except for the 18 valence electrons were used for the three metals Ni, Pd, and Pt. For Sn, the double-ζ valence basis functions with a 5d polarization function with the exponent 0.183[13] and the Hay−Wadt ECP[11] to replace the core electrons except for the four valence electrons were used.

All equilibrium and transitions state structures were fully optimized without any symmetry restriction unless otherwise indicated and identified by the number of imaginary frequencies calculated from the analytical Hessian matrix. All the reaction coordinates were followed from the transition state to the reactant and the product by the intrinsic reaction coordinate (IRC) technique.[14] NBO analysis[15] was performed to obtain the atomic orbital (AO) population and the charge. The energies relative to the (iminophosphine)M (M = Ni, Pd, Pt) complexes **1** and the free $SnH_3C{\equiv}CH$ and benzyne are presented.

3. Results and Discussion

3.1. Cycle A. As mentioned in the Introduction, the first step of cycle A is the oxidative addition of the Sn−C σ-bond of $SnH_3C{\equiv}CH$ to the palladium(0)−iminophosphine complex **1**. The vacant site on complex **1** is already activated by the small ∠P−Pd−N bite angle of 104.0°. The vacant sp-hybridized orbital in the P−Pd−N plane is stabilized, whereas the occupied dπ orbital in the P−Pd−N plane is destabilized and is well-known[16] to interact with the σ and the σ* orbitals of the Sn−C bond by electron donation and back-donation. The ∠P−Pd−N bite angle of **1** becomes even smaller to enhance the activity of these occupied and unoccupied orbitals of the Pd when the substrate interacts with the Pd (see Figure 2). The incoming $SnH_3C{\equiv}CH$ forms the stable C≡C π-complex first interacting with the Pd before the Sn−C σ-bond cleavage. Starting from the C≡C π-complex, the activation of the Sn−C σ-bond of $SnH_3C{\equiv}CH$ occurs in the ∠P−Pd−N plane by the parallel approach of the Sn−C σ-bond to the ∠P−Pd−N plane, although the author has reported Sn−C σ-bond activation by the perpendicular approach on the phosphine-coordinate palladium complex.[7] This distinct difference is ascribed to the electronic effect of the N−P hybrid ligand and the small bite angle of the chelate ligand, as discussed in detail in a previous paper.[17]

Two pathways, **2** → **TS1** → **3** and **2′** → **TS1′** → **3′**, are considered taking account of the position of the P and the N ligands. The C^2 atom is cis to the N ligand in the former while trans in the latter. One would notice that the trans influence of the weakly σ-donative P ligand[17] is reflected on the Pd−C distances in the C≡C π-complexes **2** and **2′**. The Pd−C^1 distance is 0.008 Å longer in **2′** than in **2**. On the other hand, the Pd−C^2 distance is 0.014 Å longer in **2** than in **2′**. These facts are reasonable because the weak σ-donation of the P ligand affects and reduces the electron back-donation to the π* orbitals of $C^1{\equiv}C^2$. As a result, the Pd−C bond trans to the P ligand is more weakened. Another trend should also be noted. The localized electron on the C^1 atom due

(3) Sahnoun, R.; Matsubara, T.; Yamabe, T. *Organometallics* **2000**, *19*, 5661.
(4) Matsubara, T.; Hirao, K. *Organometallics* **2002**, *21*, 1697.
(5) Matsubara, T.; Hirao, K. *J. Am. Chem. Soc.* **2002**, *124*, 679.
(6) Matsubara, T.; Hirao, K. *Organometallics* **2002**, *21*, 2662.
(7) Matsubara, T.; Hirao, K. *Organometallics* **2002**, *21*, 4482.
(8) Frisch, M. J.; Trucks, G. W.; Schlegel, H. B.; Scuseria, G. E.; Robb, M. A.; Cheeseman, J. R.; Zakrzewski, V. G.; Montgomery, J. A., Jr.; Stratmann, R. E.; Burant, J. C.; Dapprich, S.; Millam, J. M.; Daniels, A. D.; Kudin, K. N.; Strain, M. C.; Farkas, O.; Tomasi, J.; Barone, V.; Cossi, M.; Cammi, R.; Mennucci, B.; Pomelli, C.; Adamo, C.; Clifford, S.; Ochterski, J.; Petersson, G. A.; Ayala, P. Y.; Cui, Q.; Morokuma, K.; Malick, D. K.; Rabuck, A. D.; Raghavachari, K.; Foresman, J. B.; Cioslowski, J.; Ortiz, J. V.; Stefanov, B. B.; Liu, G.; Liashenko, A.; Piskorz, P.; Komaromi, I.; Gomperts, R.; Martin, R. L.; Fox, D. J.; Keith, T.; Al-Laham, M. A.; Peng, C. Y.; Nanayakkara, A.; Gonzalez, C.; Challacombe, M.; Gill, P. M. W.; Johnson, B. G.; Chen, W.; Wong, M. W.; Andres, J. L.; Gonzalez, C.; Head-Gordon, M.; Replogle, E. S.; Pople, J. A. *Gaussian 98*; Gaussian, Inc.: Pittsburgh, PA, 1998.
(9) (a) Lee, C.; Yang, W.; Parr, R. G. *Phys. Rev. B* **1988**, *37*, 785. (b) Becke, D. *J. Chem. Phys.* **1993**, *98*, 5648.
(10) Hay, P. J.; Wadt, W. R. *J. Chem. Phys.* **1985**, *82*, 299.
(11) Wadt, W. R.; Hay, P. J. *J. Chem. Phys.* **1985**, *82*, 284.
(12) Ehlers, A. W.; Böhme, M.; Dapprich, S.; Gobbi, A.; Höllwarth, A.; Jonas, V.; Köhler, K. F.; Stegmann, R.; Veldkamp, A.; Frenking, G. *Chem. Phys. Lett.* **1993**, *208*, 111.
(13) Huzinaga, S. *Physical Sciences Data 16, Gaussian Basis Sets for Molecular Calculations*; Elsevier: Amsterdam, 1984.
(14) Fukui, K.; Kato, S.; Fujimoto, H. *J. Am. Chem. Soc.* **1975**, *97*, 1.
(15) Glendening, E. D.; Reed, A. E.; Carpenter, J. E.; Weinhold, F. *NBO Version 3.1*.
(16) Ref 7 and references therein.
(17) Matsubara, T. *Organometallics*, in press.

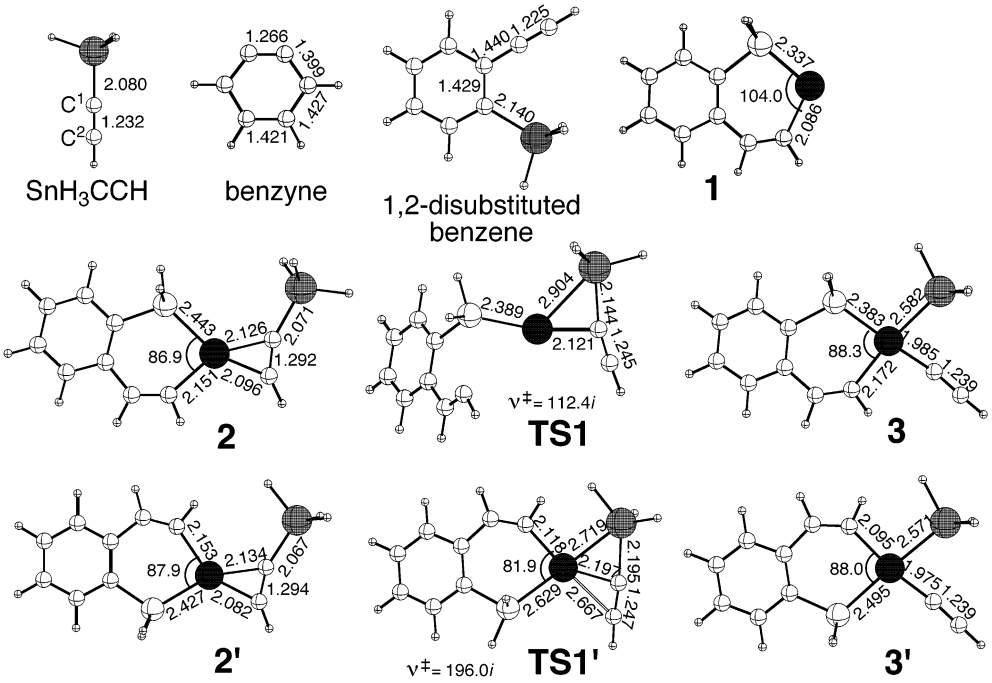

Figure 2. B3LYP/BSI-optimized structures (in Å and deg) of the starting complex (**1**), the intermediates (**2**, **2′**, **3**, **3′**), and the transition states (**TS1**, **TS1′**) involved in cycle A, together with the free $SnH_3C{\equiv}CH$, benzyne, and 1,2-disubstituted benzene (product). The imaginary frequencies (in cm^{-1}) are shown for transition states **TS1** and **TS1′**.

Table 1. NBO Analysis of the Free $XH_3C^1{\equiv}C^2H$ (X = C, Si, Ge, Sn) at the B3LYP/BSI Level

	atomic charge			X−C¹ σ-bond % X	C¹-C² σ-bond % C¹	C¹-C² π-bond % C¹
	X	C¹	C²			
C	−0.696	−0.009	−0.256	50.2	50.2	49.6
Si	0.860	−0.479	−0.164	29.5	49.9	51.8
Ge	0.930	−0.486	−0.178	28.6	49.6	51.6
Sn	1.220	−0.548	−0.187	24.7	49.4	51.4

to the high polarization of the Sn−C^1 bond weakens the electron back-donation from the Pd to the C^1 atom. The Pd−C^1 distance is, therefore, longer than the Pd−C^2 distance in both **2** and **2′**. The steric repulsion between the bulky SnH_3 substituent and the ligand would also promote this trend.

The electron-rich C^1 atom slightly slides on the P−Pd−N plane to sufficiently interact with the unoccupied sp-hybridized orbital of the Pd by the electron donation. Since the Sn−C σ-bond is highly polarized and the electron is localized on the C^1 atom (see Table 1), the C^1 atom dominantly contributes to this electron donation. The Pd−C^1 distances in **2** and **2′** are kept short during the approach of the Sn−C σ-bond to the Pd by the participation of the π orbital of the C^1 atom in the electron donation. Thereby, the angle ∠Sn−C^1−C^2 is not reduced so much in the transition state. After the electron donation from the Sn−C σ orbital to the valence sp-hybridized orbital of Pd, electron back-donation from the dπ orbital of Pd on the P−Pd−N plane to the σ* orbital of the Sn−C bond takes place. Here, the highly positively charged Sn atom is located on the top of the lobe of the dπ orbital on the P−Pd−N plane in the transition states **TS1** and **TS1′** to sufficiently receive the electron. Nevertheless, the N ligand dissociates from Pd in the transition state **TS1**, since the character of the N ligand that is strongly σ-donative causes electronic repulsion with the occupied dπ orbital of Pd. In contrast, when the activation of the Sn−C σ-bond starts from **2′**, the Pd−N distance becomes rather shorter in the transition state **TS1′**. The electron back-donation from Pd to the π* orbital of the C^2 atom, which is responsible for the short Pd−C^2 distance of 2.667 Å, would reduce the electronic repulsion between the N ligand and the Pd. Since the C^2 atom is attracted to Pd in the transition state **TS1′** by electron back-donation, the dissociation of the C^2 and the association of Sn occur competitively. The same phenomenon has been found in the Sn−C σ-bond activation in the $(PH_3)(NH_3)Pd + SnH_3C{\equiv}CH$ and the $(NH_2C_2H_4NH_2)Pd + SnH_3C{\equiv}CH$ systems.[17] Any interaction and reaction of the second substrate, benzyne, was not found for both **3** and **3′** despite the careful search.

The potential energies of two paths, **2** → **TS1** → **3** and **2′** → **TS1′** → **3′**, are presented in Table 2. Although the energies of the C≡C π-complexes and the activation products of the two paths are nearly the same, the transition state is 7.1 kcal/mol more stable for **TS1** than for **TS1′**. This is reasonably understood from the structures of the two transition states, which are obviously different. The coordinated $SnH_3C{\equiv}CH$ in the transition state **TS1′** is not allowed to sufficiently relax due to the strong binding of the C^2 atom to Pd mentioned above. The Sn−C^1−C^2 axis is still kept linear in **TS1′**, although the Sn−C σ-bond is stretched to 2.195 Å. This restriction of the motion of the coordinated $SnH_3C{\equiv}CH$ causes the destabilization of the transition state **TS1′**. The potential energy surface of path **2** → **TS1** → **3** of cycle A (path a) was much higher in energy than those of paths b and c of cycle B as presented in Figure 3, which suggests that cycle B is thermodynamically more favorable than cycle A.

3.2. Cycle B. The coordination of the C≡C triple bond of aryne to the palladium(0)−iminophosphine complex **1** is the first step in cycle B. In the formed π-complex **4**,

Downloaded by CARLI CONSORTIUM on June 29, 2009
Published on September 16, 2003 on http://pubs.acs.org | doi: 10.1021/om0304053

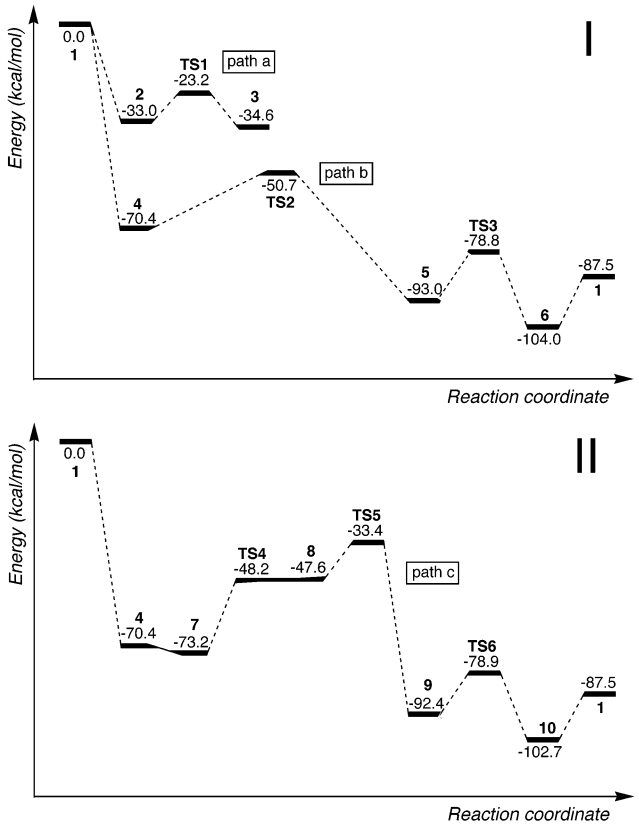

Figure 3. B3LYP/BSII potential energy surfaces (in kcal/mol) of the carbostannylation of benzyne by the palladium(0)−iminophosphine catalyst **1**. (I) path a: **1** → **2** → **TS1** → **3**; path b: **1** → **4** → **TS2** → **5** → **TS3** → **6** → **1**. (II) path c: **1** → **4** → **7** → **TS4** → **8** → **TS5** → **9** → **TS6** → **10** → **1**.

Table 2. Relative Energies (in kcal/mol) of the Equilibrium Structures and the Transition States Involved in the Catalytic Cycle of the Carbostannylation of Benzyne by the Palladium(0)−Iminophosphine Complex 1 at the B3LYP/BSI and the B3LYP/BSII Levels

	B3LYP/BSI	B3LYP/BSII		B3LYP/BSI	B3LYP/BSII
1	0.0	0.0			
2	−32.0	−33.0	**2′**	−32.4	−33.3
TS1	−19.5	−23.2	**TS1′**	−17.9	−16.1
3	−35.3	−34.6	**3′**	−36.1	−33.3
4	−72.1	−70.4			
TS2	−52.6	−50.7	**TS2′**	−47.3	−43.4
5	−97.5	−93.0			
TS3	−81.3	−78.8			
6	−104.2	−104.0			
7	−69.4	−73.2	**7′**	−64.8	−63.7
TS4	−47.4	−48.2	**TS4′**	−48.4	−48.0
8	−49.4	−47.6	**8′**	−48.8	−48.3
TS5	−33.7	−33.4	**TS5′**	−30.1	−28.2
9	−97.8	−92.4			
TS6	−81.4	−78.9			
10	−103.2	−102.7			
1	−87.8	−87.5			

the Pd−C bond trans to the P ligand is longer than that trans to the N ligand (Figure 4), as mentioned above for **2** and **2′**. From the benzyne π-complex **4**, two independent paths, **4** → **TS2** → **5** → **TS3** → **6** → **1** and **4** → **7** → **TS4** → **8** → **TS5** → **9** → **TS6** → **10** → **1**, were found (paths b and c, respectively, in Figure 3). In both paths b and c, the Sn−C bond breaking of $SnH_3C{\equiv}CH$ and the migration of SnH_3 to the C atom of the benzyne C≡C take place first, and then the counterpart C≡CH couples with the other C atom of the benzyne C≡C to produce the 1,2-disubstituted benzene. The essential difference between paths b and c is found in the mechanism of the Sn−C bond breaking of $SnH_3C{\equiv}CH$. The Sn−C σ-bond is broken by the oxidative addition of the Sn−C σ-bond to the Pd in path c, while it is broken without the oxidative addition to the Pd in path b. However, the apical site of the Pd complex plays an important role in both paths. This is very interesting because the contribution of the apical site of the d^{10} Pd(0) complex to the catalytic reaction is little known.

The Sn atom of the second substrate $SnH_3C{\equiv}CH$ approaches one of the C≡C carbons of the coordinated aryne, and the $C^1{\equiv}C^2$ of $SnH_3C{\equiv}CH$ occupies the apical position in the transition state **TS2** of path b. Here, the Pd−C(benzyne) bond length is elongated and the Sn atom migrates to the C(benzyne) atom without coordination to the Pd. On the other hand, C^1 of the $C^1{\equiv}C^2H$ counterpart as well as one of the C(benzyne) atoms coordinates to Pd in the equatorial position to form the complex **5**. Pd(0) is finally oxidized to Pd(II) in **5**.

The Sn−C bond breaking in the step from **4** to **5** is considered to be heterolytic. As presented below, the Sn−C bond of $SnH_3C{\equiv}CH$ is still highly polarized in the transition state **TS2**. The Pd atom in **4** has a positive

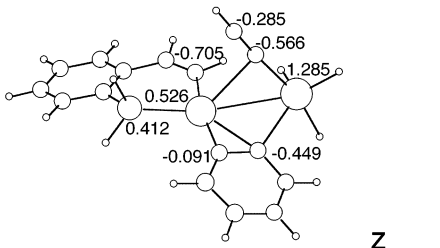

TS2

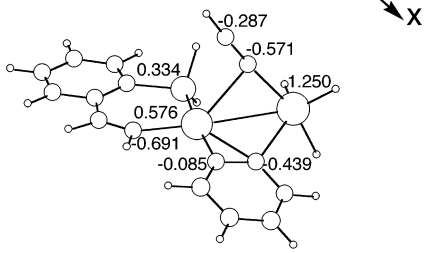

TS2'

charge of 0.384 e due to electron back-donation from the occupied Pd dπ orbital to the benzyne C≡C π* orbital. This positive charge of the Pd atom increases to 0.526 e in **TS2**, although one of the Pd−C distances is largely lengthened to 2.405 Å. Here, we notice that there exist two important flows of an electron in **TS2**. The electron of the Pd is transferred to the C^1 of $SnH_3C{\equiv}CH$ and the C^3 of the benzyne C≡C as illustrated below.

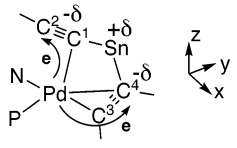

The transition state **TS2** is stabilized in energy and the Sn of $SnH_3C{\equiv}CH$ comes closer to the benzyne C≡C

Downloaded by CARLI CONSORTIUM on June 29, 2009
Published on September 16, 2003 on http://pubs.acs.org | doi: 10.1021/om0304053

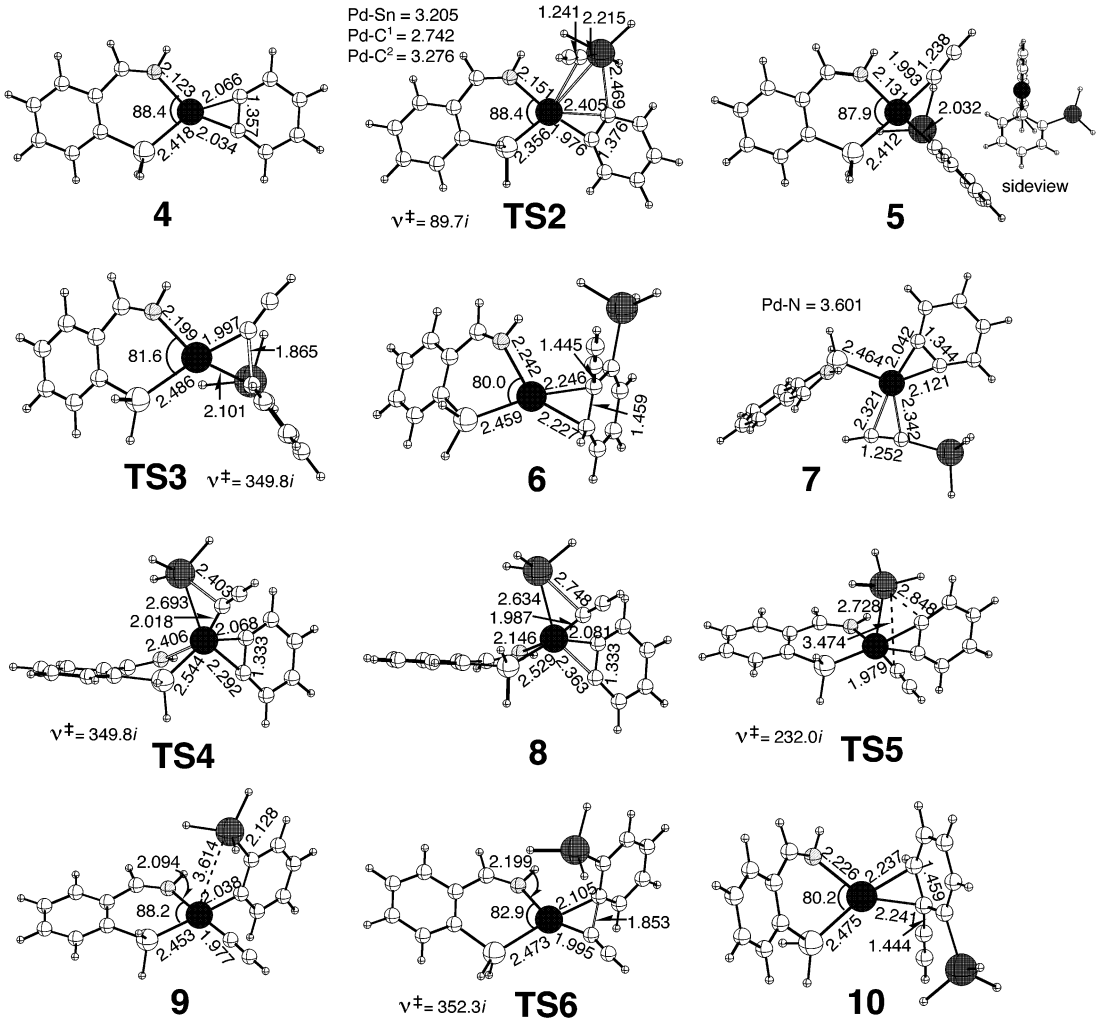

Figure 4. B3LYP/BSI-optimized structures (in Å and deg) of the intermediates (**4**−**10**) and the transition states (**TS2**−**TS6**) involved in paths b and c of cycle B. The imaginary frequencies (in cm^{-1}) are shown for the transition states **TS2**−**TS6**.

carbon by the attractive interaction between the Pd and C^1 by electron back-donation from the Pd d orbital to the C^1 π^* orbital. In fact, the populations of the occupied d_{z^2}, d_{yz}, and d_{xz} orbitals of the Pd are all reduced to 1.900−1.945 e. On the other hand, the total charge of $SnH_3C{\equiv}CH$ increases to −0.263 e, and the transferred electron is accumulated on the C^2 atom. The total negative charge of the benzyne in **4** (−0.565 e) also slightly increases in **TS2** (−0.574 e), although the electron back-donation to the benzyne C≡C π^* orbital is significantly weakened by the stretch of the Pd−C^4 bond. The electron transferred from the Pd is largely localized on the C^4 atom to receive the positively charged Sn. The electron flow from the Pd to C^4 along the Pd−C^3−C^4 linkage is promoted by the strongly electron-donative N ligand trans to C^3. Therefore, it is reasonable to consider that the highly polarized Sn−C σ-bond of $SnH_3C{\equiv}CH$ is heterolytically broken and the highly positively charged Sn is transferred to the highly negatively charged C^4 atom. The positive charge of the Sn and the negative charge of the C^4 do not change so much in **5**, since the Sn−C^4 bond in **5** is also highly polarized. The highly negatively charged C^3 and C^1 by the electron received from the Pd coordinate to Pd in the equatorial plane in **5**. Thus, Pd(0) is oxidized to Pd(II) in **5**. A similar transition state was not found for $XH_3C{\equiv}CH$ (X = C, Si, Ge), which have the less polarized X−C bond.

It is easily predicted that the electron flow from Pd to C^4 along the Pd−C^3−C^4 linkage is reduced when the positions of the N and the P ligands are mutually switched. The total negative charge of the benzyne and the negative charge on C^4 decrease in **TS2′** as expected. The total negative charge of the benzyne and the negative charge on C^4 were −0.561 e and −0.439 e, respectively, in **TS2′**. Therefore, the migration of the Sn to C^4 by heterolytic cleavage of the Sn−C^1 bond would be depressed. This is reflected in the energy of the transition states **TS2** and **TS2′**, the energy of **TS2′** being higher by 7.3 kcal/mol than that of **TS2** (Table 2). The influence of the N ligand also appears in the geometry. The Pd−C^1 distance of 2.602 Å in **TS2′** (Figure 5) is shorter by 0.140 Å than that in **TS2**. The interaction of C^1 with the Pd is strengthened in **TS2′** because the electron back-donation from the Pd to the π^* orbital of C^1 is enhanced by the strongly electron-donative N ligand. The 1,2-disubstituted benzene is produced from **5** by the C−C coupling through the transition state **TS3**.

In path c, the oxidative addition of the Sn−C σ-bond of $SnH_3C{\equiv}CH$ occurs in **4**. The weakly bound nitrogen ligand[17] dissociates and the C≡C π-bond of $SnH_3C{\equiv}CH$

Downloaded by CARLI CONSORTIUM on June 29, 2009
Published on September 16, 2003 on http://pubs.acs.org | doi: 10.1021/om0304053

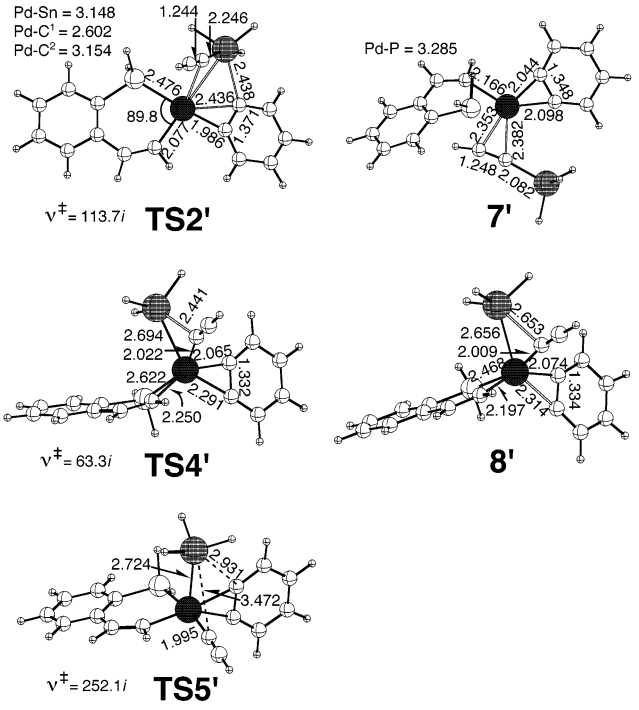

Figure 5. B3LYP/BSI-optimized structures (in Å and deg) of the intermediates (**7′**, **8′**) and the transition states (**TS2′**, **TS4′**, **TS5′**) involved in cycle B. The imaginary frequencies (in cm^{-1}) are shown for the transition states **TS2′**, **TS4′**, and **TS5′**.

coordinates to the prepared vacant site to form **7**. The coordinated $SnH_3C{\equiv}CH$ and benzyne in **7** rotate to make the Sn−C σ-bond and the C≡C π-bond perpendicular to the equatorial plane, where the N ligand recoordinates to the Pd. In the formed intermediate **8** passing through the transition state **TS4**, the Pd−Sn distance is shortened to 2.634 Å, and the Sn−C distance is largely stretched to 2.748 Å. The Pd−C^1 distance is kept short during the reaction, which is similar to the case of path a. The reaction further proceeds passing through the transition state **TS5**. The structure becomes a five-coordinate square-pyramid in **TS5**, where the Sn occupies the apical position. After passing through the transition state **TS5**, the Sn migrates to the carbon of the coordinated benzyne C≡C in the equatorial position to form the intermediate **9**. The C−C coupling occurs in **9** to form the 1,2-disubstituted benzene through the transition state **TS6**.

The back-donated electron from Pd is uniformly distributed in the C≡C of the coordinated benzyne in the transition state **TS5**, as displayed below.

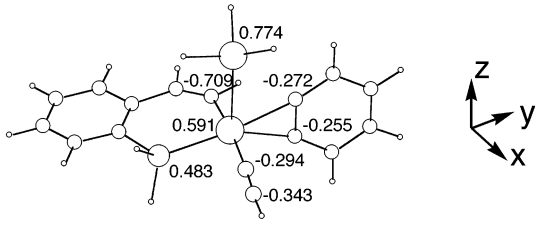

TS5

The positive charge of the coordinated Sn at the apical position significantly decreases to 0.774 e, suggesting the oxidative addition of the Sn−C σ-bond by the homolytic cleavage. The electron back-donation for the oxidative addition of the Sn−C σ-bond would be encouraged when the strongly electron-donative N ligand is trans to the C^1 of $SnH_3C^1{\equiv}C^2H$. This is explicitly reflected in the energies of the transition states **TS5** and **TS5′**; the transition state **TS5**, where the N ligand is trans to C^1, is 5.2 kcal/mol more stable than the transition state **TS5′**, where the N ligand is cis to C^1, as shown in Table 2. The electron that contributes to the Pd−Sn bonding flows to the C^3 atom through the C^4 atom to complete the coordination of C^3 in the intermediate **9**.

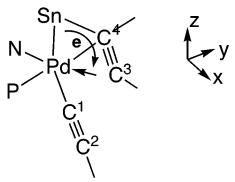

A similar transition state was also found for $XH_3C{\equiv}CH$ (X = C, Si, Ge), which have the less polarized X−C bond in contrast to the case of path b.

The entire potential energy surfaces of paths b and c are presented in Figure 3. A large energy barrier exists for the Sn−C bond breaking of $SnH_3C{\equiv}CH$ in both paths b and c, which indicates that this step is rate-determining. The resting state **8** between **7** and **TS5** disappears at the higher B3LYP/BSII level, although the resting state **8′** between **7′** and **TS5′** does not (see Table 2). The energy barriers of the C−C coupling in the last step of paths b and c are small, and the shape of the potential energy surfaces is nearly the same. Since the highest point at **TS2** of path b is lower in energy than that at **TS5** of path c and the energy barrier is smaller for path b than for path c, path b is considered to be thermodynamically and kinetically more favorable than path c. However, if the Pd atom of complex **1** is replaced by the Pt atom, which is more easily oxidized from Pt(0) to Pt(II),[18] this path preference would be changed.

In answer to this assumption, the transition states **TS2pt**, **TS2′pt**, **TS5pt**, and **TS5′pt** for Pt were optimized and their energies were calculated. These results are presented in Figure 6 and Table 3 together with those for Ni. The features of the optimized structures for Ni and Pt are almost the same as those for Pd. The influence of the N ligand was also similarly found in the geometric parameters and the energies. However, the trend in the energies of **TS2** and **TS5** was changed for Pt as expected. The transition state **TS5** is lower in energy than the transition state **TS2**. This suggests that path c, with oxidative addition of the Sn−C σ-bond of $SnH_3C{\equiv}CH$ to Pt, is energetically more favorable than path b, without the oxidative addition of the Sn−C σ-bond of $SnH_3C{\equiv}CH$ to Pt in the case of Pt.

4. Concluding Remarks

The mechanism of catalytic carbostannylation of aryne by the palladium(0)−iminophosphine complex was examined by the density functional method (B3LYP)

(18) It is generally well-known that the oxidation more easily occurs in Pt than in Pd by the shielding effect.

Downloaded by CARLI CONSORTIUM on June 29, 2009
Published on September 16, 2003 on http://pubs.acs.org | doi: 10.1021/om0304053

Downloaded by CARLI CONSORTIUM on June 29, 2009
Published on September 16, 2003 on http://pubs.acs.org | doi: 10.1021/om0304053

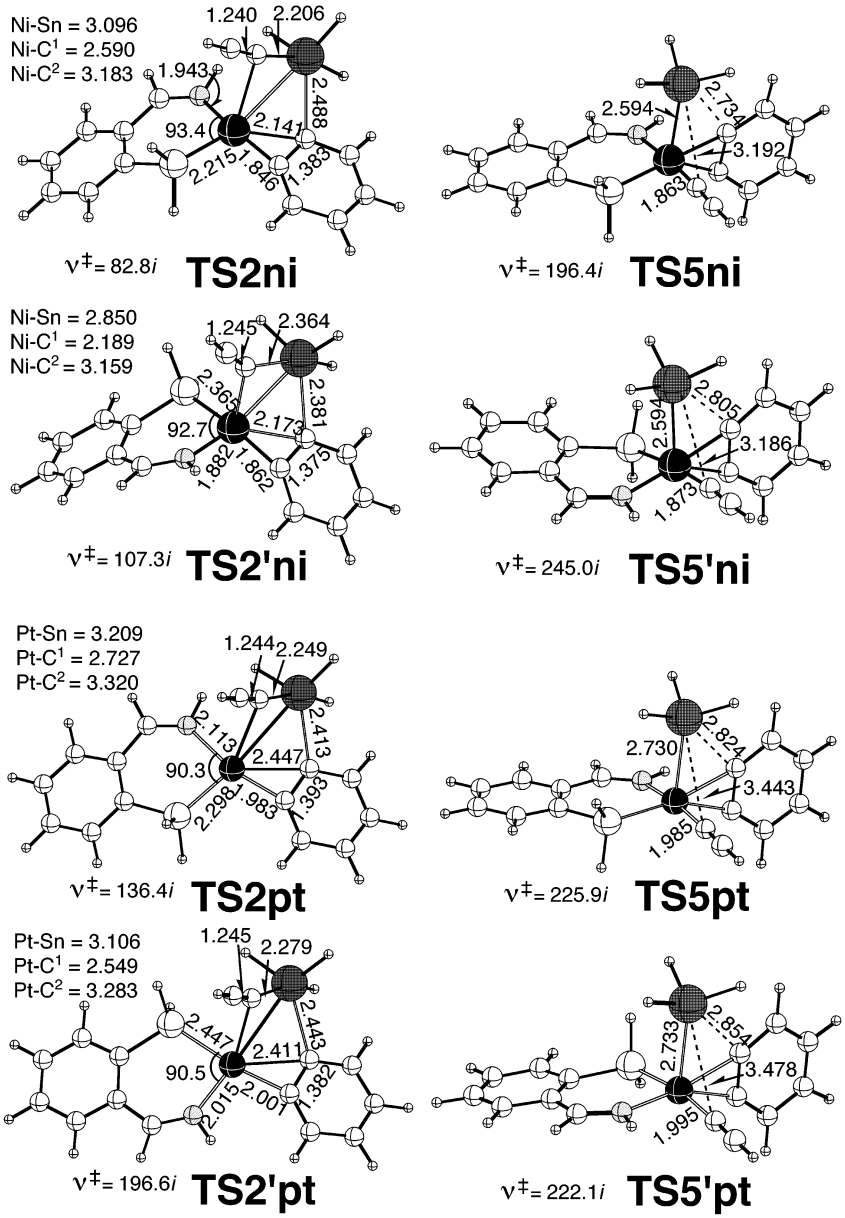

Figure 6. B3LYP/BSI-optimized structures (in Å and deg) of the transition states **TS2ni**, **TS2′ni**, **TS5ni**, and **TS5′ni** for Ni and **TS2pt**, **TS2′pt**, **TS5pt**, and **TS5′pt** for Pt involved in cycle B. The imaginary frequencies (in cm^{-1}) are shown for all the transition states.

Table 3. Energies (in kcal/mol) of the Transition States TS2ni, TS2′ni, TS5ni, and TS5′ni for Ni and TS2pt, TS2′pt, TS5pt, and TS5′pt for Pt Involved in Cycle B at the B3LYP/BSI and the B3LYP/BSII Levels[a]

	B3LYP/BSI	B3LYP/BSII		B3LYP/BSI	B3LYP/BSII
TS2ni	−69.2	−67.1	TS2′ni	−67.4	−63.3
TS5ni	−56.2	−55.5	TS5′ni	−50.0	−49.1
TS2pt	−63.4	−62.7	TS2′pt	−57.7	−53.4
TS5pt	−64.9	−65.7	TS5′pt	−63.3	−61.7

[a] Energies relative to the starting complexes for Ni and Pt and the free $SnH_3C{\equiv}CH$ and benzyne are presented.

paying attention to the role of the apical site. The model substrates $SnH_3C{\equiv}CH$ as alkynylstannane and benzyne as aryne and the model iminophosphine ligand were adopted for the computation. The calculations showed that the catalytic reaction takes cycle B out of two possible cycles A and B (cycle A: **1** → **3** → **1**; cycle B: **1** → **4** → **1**). It is quite interesting that the apical site plays an important role in both paths in cycle B, alternative paths b and c existing in cycle B. This is the first case to reveal the contribution of the apical site of the d^{10} Pd(0) complex to the catalysis as far as the author's knowledge, although the author has suggested the importance of the apical site of the d^{10} Pd(0) complex on the elementary reactions.[3−7] The apical site is an origin of the catalysis of the palladium(0)−iminophosphine complex **1**, and the contribution of the apical site makes the catalytic reaction possible in cycle B. The energy barrier of the rate-determining step, the Sn−C σ-bond breaking of $SnH_3C{\equiv}CH$, is significantly lowered by the contribution of the apical site. Path b, with the heterolytic cleavage of the Sn−C σ-bond of $SnH_3C{\equiv}CH$ without the oxidative addition to Pd, was more favorable thermodynamically and kinetically than path c, with the homolytic cleavage of the Sn−C σ-bond of $SnH_3C{\equiv}CH$ by oxidative addition to Pd. However, when the Pd atom is replaced by the Pt atom, path c, with the homolytic

cleavage of the Sn−C σ-bond by oxidative addition, becomes energetically more favorable.

Acknowledgment. The calculations were in part carried out at the Computer Center of the Institute for Molecular Science, Japan.

Supporting Information Available: Listings giving the optimized Cartesian coordinates of all equilibrium structures and transition states presented in this paper. This material is available free of charge via the Internet at http://pubs.acs.org.

OM0304053

Downloaded by CARLI CONSORTIUM on June 29, 2009
Published on September 16, 2003 on http://pubs.acs.org | doi: 10.1021/om0304053